Inferring the pairing symmetry of the superconducting Sn/Si(111) via angle-resolved terahertz pump spectroscopy

Mattia Iannetti [1,2,*] Tommaso Cea [1] Cesare Tresca [1,2] Lara Benfatto [3] and Gianni Profeta [1,2]

[1] *Dipartimento di Scienze Fisiche e Chimiche, Universitá degli Studi dell'Aquila, Via Vetoio 10, I-67100 L'Aquila, Italy*

[2] *CNR-SPIN C/o Dipartimento di Scienze Fisiche e Chimiche, Universitá Degli Studi dell'Aquila, Via Vetoio 10, I-67100 L'Aquila, Italy*

[3] *Department of Physics, Sapienza University of Rome, P.le A. Moro 2, 00185 Rome, Italy*

(Received 12 December 2023; revised 15 December 2025; accepted 14 January 2026; published 2 February 2026; corrected 23 February 2026)

Doping tin surface epitaxially grown on silicon, Sn/Si(111), with boron atoms yields the appearance of a superconducting (SC) phase below $T_c \sim 4-9$ K. Even though the pairing mechanism remains unknown, experimental evidence of chiral $d-$wave superconductivity has been recently reported, thus ruling out a phonon-mediated pairing. Here, we study theoretically the SC phase of the doped Sn/Si(111) within a $t-J$ model investigating different symmetries of the order parameter. We analyze the photoexcitation of the system by intense terahertz pulses and show that the polarization dependence of the induced current can distinguish between different symmetries of the SC gap, thus providing an experimental means to investigate the spectroscopic features of the Sn/Si(111), and possibly to many other systems, across the SC transition.

DOI: 10.1103/p357-5pth

I. INTRODUCTION

The α phase of monolayer group-IV elements epitaxially grown on semiconducting surfaces provides a surprisingly rich platform to study the competition between strongly correlated phenomena, spin transport, and lattice reconstruction. One-third monolayer coverage of heavy atoms, like Sn and Pb, displays an isoelectronic $\sqrt{3}\times\sqrt{3}R30^\circ$ reconstruction, where the host atoms, the adatoms, occupy the T_4 site in a triangular lattice [1], which is called the α phase. The three dangling bonds at the surface of the substrate saturate with the adatoms, leaving a free electron at each T_4 site to form a half-filled surface band within the substrate's band gap. Such a surface band gets strongly affected by the electronic interactions. Some materials, like Pb/Ge(111), Sn/Ge(111), and Pb/Si(111), exhibit a low-temperature 3×3 lattice reconstruction, yielding a charge-density wave, which is often metallic [2–9]. In contrast, Sn/Si(111) displays a low-temperature Mott insulating phase [2,4,10,11], with the possible development of a $2\sqrt{3}\times\sqrt{3}$ collinear antiferromagnetic (AFM) phase [11–13], not yet clearly observed experimentally. A renewed interest in the study of these systems has been recently provided by the discovery of superconductivity in the Sn/Si(111) hole doped with boron [14], with critical temperatures of the order of $T_c \sim 4-9$ K. Even though the pairing mechanism is still an open question, it is believed that Sn/Si(111) displays unconventional superconductivity of electronic origin, driven by the nonlocal Coulomb interactions [4,15,16]. Reference [17] recently found experimental evidence of chiral $d-$wave superconductivity, ruling out (i) a conventional phonon-mediated pairing and (ii) the presence of a spin-triplet superconducting (SC) order parameter (OP). In the past years, some theoretical works have reported different results on the electron-phonon coupling, ranging from large [14,18] to low [15,16,19] values, but a conclusive full first-principles calculation is still missing. Up to now, the Quasi Particle Interference (QPI) spectra in Ref. [17] are the only experimental evidence of the gap symmetry.

Moreover, the chiral SC pairing is generally favored in triangular lattice systems, which are naturally prone to break the time-reversal symmetry, as it has been studied in graphene-based materials [20,21] and in other systems, like water intercalated sodium cobaltates [22]. However, the gap symmetry of the ground state strongly depends on many parameters such as doping and exchange interactions and may exhibit complex quantum phase diagrams [23,24].

The present state of the art challenges a deeper understanding of the nature of the SC pairing observed in the Sn/Si(111) and the engineering of new experimental protocols to determine the symmetry of the SC gap.

In the last years, the use of intense terahertz (THz) light pulses either in pump-probe protocols or for high-harmonic generation offered a powerful tool to address the physics of several SC systems [25–27]. Exploiting the nonlinear light-matter interaction, this technique allows one to resonantly excite the low-energy modes of the superconductor and track their dynamics in the time domain. The lowest-order nonlinear effect induced by the incident light in centrosymmetric systems is the third-harmonic generation (THG), which can be strongly enhanced in the SC phase when the frequency of

*Contact author: mattiaiannetti@gmail.com

Published by the American Physical Society under the terms of the Creative Commons Attribution 4.0 International license. Further distribution of this work must maintain attribution to the author(s) and the published article's title, journal citation, and DOI.

the light lies in the neighboring of the SC gap Δ [28–42]. In addition, the measured dependence of the nonlinear response on the light polarization with respect to the main crystallographic axes [29,30,34,35] can provide additional information on the form of the pairing interaction [43], on the disorder level [44–46], and on the symmetry of the SC OP [47]. So far, nonlinear THz photoexcitation has been intensively used to probe both conventional BCS superconductors, like NbN [28,29,38], Nb_3Sn [31,33], and MgB_2 [32,37,39], and unconventional high $-T_c$ cuprate [30,34,41,42,48] and pnictide [36,40] superconductors.

In this paper we study theoretically the superconductivity in the doped Sn/Si(111), assuming that the interactions responsible for the pairing are of AFM nature. To this purpose we first work within the $t-J$ model, which we characterize for the physical system Sn/Si(111), determining its energy parameters by the direct comparison with both first-principles calculations and the experimental data; then, we further explore extended gap symmetries.

At the mean-field (MF) level, we find two almost degenerate ground states (GSs), one with chiral $d_{x^2-y^2}+id_{xy}$-wave symmetry and the other with nematic d wave (that could be stabilized for some parameters in the quantum phase diagram of the correlated triangular lattice [23,24]), the latter breaking the C_3 symmetry out of C_6. By computing the nonlinear current induced by a THz light pulse as a function of the polarization of the incident light, we show that the THG is $\pi/3$ periodic for the $d_{x^2-y^2}+id_{xy}$ wave and π periodic for the nematic d wave. We then broaden our study to p- and f-wave states to compute the THG response in other plausible gap symmetries that can arise, e.g., at different doping regimes, as described in Refs. [15,23,24], finding that the polarization dependence of the THG is sensible to the symmetry of the modulus of the superconducting gap. Thus, our work proposes the angle-resolved THz pump spectroscopy as an experimental tool to discriminate the symmetry of the SC OP in the Sn/Si(111) and possibly in many other systems, alternatively or complementary to other spectroscopic techniques based on the quasiparticle interference [17,49].

II. THE MODEL FOR SUPERCONDUCTIVITY

As the superconductivity in Sn/Si(111) emerges by doping a half-filled AFM Mott insulator, we model the Hamiltonian of the free bond of the Sn atoms on the T_4 sites within the $t-J$ model:

$$H = H_{tb} + H_J, \tag{1}$$

where

$$H_{tb} = \sum_{ij\sigma}(t_{ij}-\mu\delta_{ij})c^\dagger_{i\sigma}c_{j\sigma} \tag{2}$$

is the tight-binding Hamiltonian, i, j label the sites of the triangular network, t_{ij} are the hopping amplitudes, μ is the chemical potential, and $c_{i\sigma}$ is the operator for the annihilation of one electron in the site i with spin σ. We consider hopping up to the 6th-nearest neighbor, with the corresponding amplitudes fitted from first-principles calculations (see Supplemental Material [50]). We model the additional interaction Hamiltonian, H_J, as an AFM exchange term:

$$H_J = J\sum_{\langle i,j\rangle}\left(\boldsymbol{S}_i\cdot\boldsymbol{S}_j-\frac{1}{4}\hat{n}_i\hat{n}_j\right), \tag{3}$$

with $J>0$. The sum runs over all the pairs of nearest-neighbor sites, $\boldsymbol{S}_i=\frac{1}{2}\sum_{\sigma\sigma'}c^\dagger_{i\sigma}\boldsymbol{\tau}_{\sigma\sigma'}c_{i\sigma'}$ is the spin operator, $\boldsymbol{\tau}=(\tau^x,\tau^y,\tau^z)$ are the Pauli matrices, $\hbar=1$, and $\hat{n}_i=\sum_\sigma c^\dagger_{i\sigma}c_{i\sigma}$ is the local number operator. The $t-J$ Hamiltonian (1) has been intensively studied in the last decades as a model for superconductivity in the high $-T_c$ cuprate superconductors [51–57] and in correlated electrons on a triangular lattice [58–63], which paradigmatically feature the competition between the Mott insulating and the SC phase. Indeed, besides providing a natural model for AFM ordering it can also describe unconventional superconductivity emerging out of repulsive electronic interactions. Recently, extended $t-J$ models have been exploited to describe topological SC states in triangular lattices [23,24,64].

In the absence of the electromagnetic perturbation, we perform the MF approximation to H in both the particle-hole and the particle-particle (pairing) channels (see Supplemental Material [50] for details). This procedure leads to the following quadratic Hamiltonian, expressed in the reciprocal space:

$$H^{\mathrm{MF}}_{tJ} = \sum_{\boldsymbol{k}}\left[\sum_\sigma \xi_{\boldsymbol{k}}c^\dagger_{\boldsymbol{k}\sigma}c_{\boldsymbol{k}\sigma}+(\Delta_{\boldsymbol{k}}c^\dagger_{\boldsymbol{k}\uparrow}c^\dagger_{-\boldsymbol{k}\downarrow}+\mathrm{H.c.})\right]+E_0, \tag{4}$$

where $\boldsymbol{k}$ is the wave vector in the first Brillouin zone, $\xi_{\boldsymbol{k}}=\xi^0_{\boldsymbol{k}}+\delta\xi_{\boldsymbol{k}}$, $\xi^0_{\boldsymbol{k}}$ is the noninteracting band dispersion computed from the chemical potential, $\delta\xi_{\boldsymbol{k}}$ is the MF correction in the particle-hole channel, $\Delta_{\boldsymbol{k}}$ is the pairing amplitude, and E_0 is an energy constant (see Supplemental Material [50]). Both $\delta\xi_{\boldsymbol{k}}$ and $\Delta_{\boldsymbol{k}}$ can be expressed in terms of the form factors corresponding to the s, $d_{x^2-y^2}$, d_{xy} symmetries, which are the only ones allowed by the nearest-neighbor AFM interaction of Eq. (3): $\delta\xi_{\boldsymbol{k}}=\sum_\alpha\delta t_\alpha\gamma_\alpha(\boldsymbol{k})$, $\Delta_{\boldsymbol{k}}=\sum_\alpha\Delta_\alpha\gamma_\alpha(\boldsymbol{k})$, where $\gamma_s(\boldsymbol{k})=[\cos(k_xa)+2\cos(k_xa/2)\cos(k_y\sqrt{3}a/2)]/\sqrt{3}$, $\gamma_{d_{x^2-y^2}}(\boldsymbol{k})=[\cos(k_xa)-\cos(k_xa/2)\cos(k_y\sqrt{3}a/2)]\sqrt{2/3}$, $\gamma_{d_{xy}}(\boldsymbol{k})=\sqrt{2}\sin(k_xa/2)\sin(k_y\sqrt{3}a/2)$, $a=7$Å is the lattice constant, and δt_α, Δ_α are the self-consistent solutions of (see Supplemental Material [50]):

$$\delta t_\alpha = \frac{J}{2N}\sum_{\boldsymbol{k}}\gamma_\alpha(\boldsymbol{k})\xi_{\boldsymbol{k}}\tanh(E_{\boldsymbol{k}}/2T)/E_{\boldsymbol{k}}, \tag{5}$$

$$\Delta_\alpha = \frac{J}{N}\sum_{\boldsymbol{k}}\gamma_\alpha(\boldsymbol{k})\Delta_{\boldsymbol{k}}\tanh(E_{\boldsymbol{k}}/2T)/E_{\boldsymbol{k}}, \tag{6}$$

where N is the number of lattice sites, $E_{\boldsymbol{k}}=\sqrt{\xi^2_{\boldsymbol{k}}+|\Delta_{\boldsymbol{k}}|^2}$, T is the temperature, and we set $k_B=1$. Having fixed $\xi^0_{\boldsymbol{k}}$, T_c is determined by the interaction strength J, which we set in order to reproduce the experimental results of Ref. [14]: $T_c=4.8$ K and hole doping $\delta=10\%$. We obtain $J=29$ meV (see Supplemental Material [50]), which is of the same

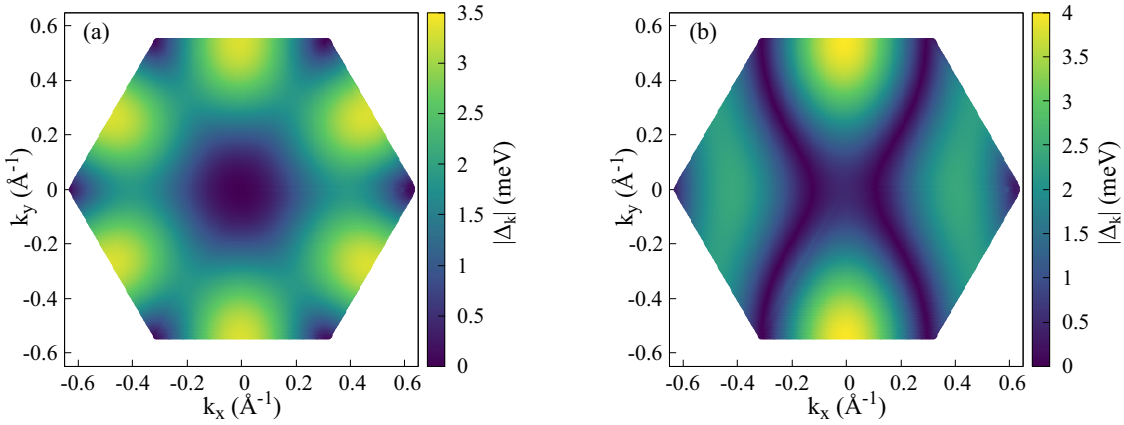


FIG. 1. Maps of $|\Delta_{\boldsymbol{k}}|$ at $T = 0$ K, for the solution with $d_{x^2-y^2} + id_{xy}$-wave symmetry (a) and with $d_{x^2-y^2}$ wave (b).

order of magnitude as that obtained by first-principles calculations [65–68]: $J_{fp} = 11$ meV. We find two distinct SC solutions (see Supplemental Material [50]), one featuring chiral $d_{x^2-y^2} + id_{xy}$-wave symmetry, as claimed in Ref. [17], and the other with nematic d-wave symmetry. We want to highlight that these two solutions are naturally obtained by selecting the initial conditions for the gap function as $\Delta^0_{d_{xy}} = i\Delta_0$, $\Delta^0_{d_{x^2-y^2}} = \Delta_0$ for the chiral d wave and $\Delta^0_{d_{xy}} \neq 0$, $\Delta^0_{d_{x^2-y^2}} \neq 0$ (but real) for the nematic d wave, where Δ_0 is a real number, without adding any constraint to the MF equations. The maps of $|\Delta_{\boldsymbol{k}}|$ at $T = 0$ K are shown in Figs. 1(a) and 1(b) for the two cases, emphasizing that the C_6 symmetry is preserved by the chiral solution, while it is broken by the nematic d wave, which only features C_2. Its is worth noting that for the nematic d-wave case, the system is symmetric under discrete rotations of $\pi/3$ in the $\Delta_{d_{x^2-y^2}} - \Delta_{d_{xy}}$ real plane (see Supplemental Material [50]). Therefore, we have chosen the initial conditions of the MF calculation in order to select the nematic $d_{x^2-y^2}$-wave symmetry (i.e., $\Delta^0_{d_{xy}} = 0$, $\Delta^0_{d_{x^2-y^2}} = \Delta_0$), which is the one shown in Fig. 1(b). The chiral symmetry is energetically favored by a very small amount: $\sim 10^{-7}$eV per site, allowing us to safely consider the two solutions as almost degenerate (see Supplemental Material [50]).

III. TRACKING THE EVOLUTION OF THE GS IN A TIME-DEPENDENT ELECTRIC FIELD

We introduce a uniform vector potential, $\boldsymbol{A}(t)$, in the Hamiltonian (4) via the Peierls substitution: $\xi^0_{\boldsymbol{k}} \to \xi^0_{\boldsymbol{k}-e\boldsymbol{A}(t)}$, where e is the electron charge and $c = 1$. It is convenient to describe the dynamics of the MF GS in terms of the quantum average of the Anderson pseudospin: $\boldsymbol{\sigma}_{\boldsymbol{k}} = \langle \Psi^\dagger_{\boldsymbol{k}} \boldsymbol{\tau} \Psi_{\boldsymbol{k}} \rangle$, where $\Psi_{\boldsymbol{k}} = (c_{\boldsymbol{k}\uparrow}, c^\dagger_{-\boldsymbol{k}\downarrow})^T$. At the MF level, $\boldsymbol{\sigma}_{\boldsymbol{k}}$ describes a precession motion given by the equations

$$\frac{d\boldsymbol{\sigma}_{\boldsymbol{k}}}{dt}(t) = 2\boldsymbol{b}_{\boldsymbol{k}}(t) \times \boldsymbol{\sigma}_{\boldsymbol{k}}(t), \tag{7}$$

with $\boldsymbol{b}_{\boldsymbol{k}} = (\Delta'_{\boldsymbol{k}}, -\Delta''_{\boldsymbol{k}}, \xi_{\boldsymbol{k}})$. Imposing $\Delta'_\alpha = -\frac{J}{N}\sum_{\boldsymbol{k}} \gamma_\alpha(\boldsymbol{k})\sigma^x_{\boldsymbol{k}}$, $\Delta''_\alpha = \frac{J}{N}\sum_{\boldsymbol{k}} \gamma_\alpha(\boldsymbol{k})\sigma^y_{\boldsymbol{k}}$, and $\delta t_\alpha = -\frac{J}{2N}\sum_{\boldsymbol{k}} \gamma_\alpha(\boldsymbol{k})\sigma^z_{\boldsymbol{k}}$, one has to solve Eq. (7) self-consistently at any time, which is equivalent to solving the Bloch equations. In this way one can track the dynamics induced by the incident field on both the gap's function, $\Delta_{\boldsymbol{k}}(t)$, and the occupation number, $n_{\boldsymbol{k}}(t)$, including all the nonlinear effects emerging for very intense fields. While $\Delta_{\boldsymbol{k}}(t)$ describes the evolution of the SC condensate, $n_{\boldsymbol{k}}(t)$ defines the electromagnetic current flowing through the sample, according to

$$\boldsymbol{J}(t) = -\sum_{\boldsymbol{k}} \nabla_{\boldsymbol{A}} \xi^0_{\boldsymbol{k}-e\boldsymbol{A}(t)} n_{\boldsymbol{k}}(t). \tag{8}$$

Experimentally, $\boldsymbol{J}$ can be measured either directly by the voltage difference at the edge of the sample, or indirectly by the electric field reflected/transmitted by the sample, though transmission measurements can be more involved due to the presence of the Si substrate and also of its phonons, which could be excited by the infrared radiation.

We want to emphasize that in the treatment of our system there are two neglected aspects that may be relevant in future theoretical works and in the experimental observation of high-harmonics generation, in particular of even harmonics. The first one is the omission of the Rashba term originating from the substrate-induced inversion-symmetry breaking in the presence of a spin-orbit coupling (SOC), due to the hybridization of the p_z band with the sp_2-like backbonds with C_3 symmetry [19]. This Rashba term is weak (and in fact neglected in other theoretical works [15,16,19]) as experimentally confirmed by angular-resolved photoemission [69,70], scanning tunneling microscopy [71–73], and spin-resolved photoemission [74]. Thus, from our tight-binding model fitted on first-principles bands obtained without SOC, the Sn p_z band should not give a contribution to even harmonics as the C_6 symmetry is preserved [19].

The second one is the possibility of light-wave driven second-harmonic generation. This effect has been seen in the centrosymmetric superconducting Nb_3Sn [33,75], and attributed to propagation effects of the nonlinear current, which can make the pump-pulse *inside* the sample nonsymmetric(i.e., $\int_{-\infty}^{\infty} dt E(t) \neq 0$). This dc component breaks inversion symmetry and allows for even higher harmonics of the pump frequency [33,75]. In the present paper we investigate the regime where propagation effects do not induce a dc component, so that the pump can be modeled with

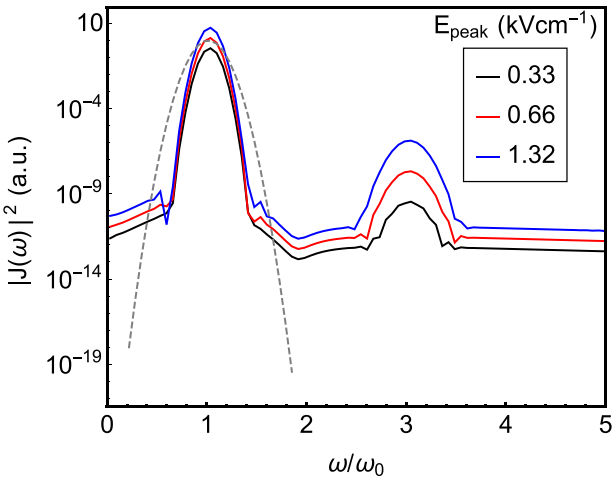


FIG. 2. Power spectrum as a function of the frequency, obtained in the chiral solution, at $T = 0$, for three different values of E_{peak}. The dashed gray line shows the power spectrum of the incident field, $|\boldsymbol{E}(\omega)|^2$. The incident field is polarized along one of the crystallographic directions.

a symmetric pulse and second-harmonic generation (SHG) is not allowed.

IV. NUMERICAL RESULTS: THE ANGLE-RESOLVED THG

The current (8) contains explicitly the response of the system at all orders in $\mathbf{A}$, since the vector potential enters both in the velocity term (gradient of the band dispersion) and in the computation of the time evolution of $n_{\mathbf{k}}(t)$. For weak field one recovers the usual linear-response result, $J^L \sim \chi^{(1)}A$, which for a purely monochromatic field at frequency ω_0 implies an induced current at the same frequency ω_0. On the other hand, for increasing strength of the driving field one can generate a nonlinear current whose lowest order scales as $J^{NL} \sim \chi^{(3)}A^3$, so that in the induced current one observes higher harmonics of the driving field, the lowest one being at $3\omega_0$. Since the THG measurements are usually performed with multicycle light pulses [28,29,34,36,37,39,41,42], which are not perfectly monochromatic, in the numerical calculations we model the vector potential as an oscillatory function at the central frequency ω_0 convoluted with Gaussian envelope $\boldsymbol{A}(t) = A_0 e^{-(t/\tau)^2} \sin(\omega_0 t)\boldsymbol{n}$, where A_0 defines the intensity of the field, τ the duration of the pulse, and $\boldsymbol{n}$ is the polarization vector, with $|\boldsymbol{n}| = 1$. Note that this vector potential defines a symmetric electric field which does not allow the light-wave SHG, safely neglected in our treatment [33,75].

Since we are interested to exploit a possible resonance of ω_0 with the gap value, we choose $\omega_0 = 1$ meV, which is of the order of $\Delta_{\boldsymbol{k}}$, and $\tau = 11$ ps, so that the frequency resolution of the pulse is $\Delta\omega/\omega_0 \simeq 0.5$. The electric field is given by $\boldsymbol{E}(t) = -\partial_t \boldsymbol{A}(t)$. Figure 2 shows the power spectrum, $|\boldsymbol{J}(\omega)|^2$, as a function of the frequency, obtained in the chiral solution, at $T = 0$, for three different intensities of the incident field, as specified in the legend, E_{peak} being the maximum of $|\boldsymbol{E}(t)|$. Here, the incident field is polarized along one of the crystallographic direction, the x axis by convention. The dashed gray line shows the power spectrum of the incident field, $|\boldsymbol{E}(\omega)|^2$. As expected, the intensity of the THG at $\omega = 3\omega_0$ increases with E_{peak} much faster than the first harmonic, the latter being dominated mostly by the linear response.

Next, we study the THG by varying the polarization of the incident field: $\boldsymbol{n} = \cos\theta\hat{x} + \sin\theta\hat{y}$. In particular, we focus on the two quantities $I^{\parallel}_{\text{THG}} = |\boldsymbol{n} \cdot \boldsymbol{J}(3\omega_0)|$ and $I^{\perp}_{\text{THG}} = |\boldsymbol{n}^{\perp} \cdot \boldsymbol{J}(3\omega_0)|$, representing the intensity of the THG in the direction parallel and orthogonal to the incident field, respectively. In the following, we will first present the THG polarization dependence of the gap symmetries that can be stabilized within our t-J model (nematic and chiral d waves); then, we extend our study also to s-, p-. and f waves as described below.

A. THG polarization response within the t-J model

Figure 3 shows $I^{\parallel}_{\text{THG}}$(a) and $I^{\perp}_{\text{THG}}$(b) as a function of θ, corresponding to $E_{\text{peak}} = 0.66\ \text{kVcm}^{-1}$ and obtained for the chiral $d_{x^2-y^2} + id_{xy}$-wave solution (red line) and for the nematic $d_{x^2-y^2}$-wave (blue line). As is evident, while $I^{\parallel}_{\text{THG}}$ is basically constant, $I^{\perp}_{\text{THG}}$ displays typical oscillations. We expect that the isotropic behavior of $I^{\parallel}_{\text{THG}}$ is mainly due to the leading contribution of the instantaneous electronic response, which is polarization independent [43]. If we then focus on $I^{\perp}_{\text{THG}}$, we note a marked difference between the two gaps' symmetries: in the chiral symmetry, $I^{\perp}_{\text{THG}}$ has a period of $\pi/3$, following from the C_6 symmetry of the crystal; in contrast, in the nematic d-wave symmetry, the period is π, as a consequence of the C_3 symmetry breaking which preserves only C_2. Therefore, the behavior of the THG as a function of the polarization of the incident field provides an experimental tool to infer the symmetry of the SC gap in the boron-doped Sn/Si(111), distinguishing between the chiral $d_{x^2-y^2} + id_{xy}$- and the nematic d wave.

B. THG polarization response for s-, p-, and f waves

We now present an extended study of the THG polarization dependence for other gap symmetries that could arise in the system upon different doping levels [15] and/or even in other systems with different parameters considering more complex Hamiltonians [23,24]. In order to do so we introduce the p- and f waves' form factors as $\gamma_p(\boldsymbol{k}) \propto \sin(k_x a) - \sin(k_x a/2)\cos(k_y\sqrt{3}a/2)$ and $\gamma_f(\boldsymbol{k}) \propto \sin(k_x a) - 2\sin(k_x a/2)\cos(k_y\sqrt{3}a/2)$. The corresponding gap functions can be computed from Eqs. (5) and (6), where now the index α is constrained to be s, p, or f depending on the gap symmetry we consider. Within this approach we can access the THG polarization response arising from different pairing symmetries, assuming their possible stabilization.

In Fig. 4 we report our results on the THG response of the parallel [Fig. 4(a)] and perpendicular [Fig. 4(b) current for s- (green line), p- (orange line) and f-wave (purple line) gap symmetries. While $I^{\parallel}_{\text{THG}}$ is dominantly constant with small modulations as in the nematic and chiral d-waves, $I^{\perp}_{\text{THG}}$ shows characteristic periodicity for the different gap functions considered. The s- and f waves have the same $\pi/3$-periodic response, while the p-wave order parameter is $\pi/2$ periodic.

Comparing these results with the nematic and chiral d waves, we can state that s-, chiral d-, and f-wave order parameters have similar THG response, resembling the C_6

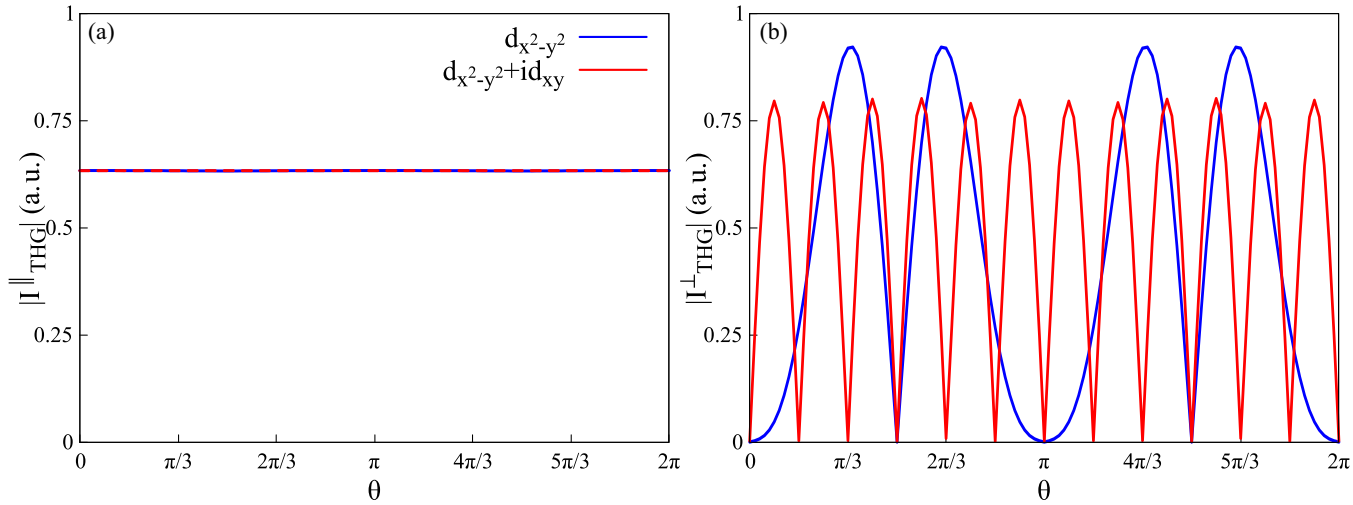


FIG. 3. $I^{\parallel}_{\mathrm{THG}}$(a) and $I^{\perp}_{\mathrm{THG}}$(b) as a function of θ, corresponding to $E_{\mathrm{peak}} = 0.66\ \mathrm{kVcm}^{-1}$ and obtained for the chiral $d_{x^2-y^2} + id_{xy}$-wave solution (red line) and for the nematic $d_{x^2-y^2}$ wave (blue line).

symmetry of the modulus of the gap function, making the optical response unable to distinguish among them. On the other hand, the p- and nematic d waves' THG polarization response is $\pi/2$- and π symmetric, respectively: while the p wave has a purely $\sim|\sin\theta|$ polarization modulation, the nematic d-wave THG contains a more complex shape. In this case, in a optical response experiment, the symmetries of these two gaps can be distinguished from the location of the peaks of $I^{\perp}_{\mathrm{THG}}$.

Thus, we can group the optical response of the superconducting Sn/Si(111) system into three classes: a first class with $\pi/6$ periodicity to which s, $d-$ chiral, and f belong; a second one with $\pi/2$ periodicity in the case of p wave; and a third one with π periodicity for the nematic d wave with complex shape.

Finally, in the experiments, the polarization dependence of I_{THG} might be sensitive to the effects of disorder [44,46], not considered here, challenging the use of ultraclean samples. Indeed, when disorder is present paramagnetic-like processes mediating the coupling of the light to SC excitations become possible, providing additional channels to generate a nonlinear response [44,46,76,77]. So far, numerical studies for square lattices have shown that these additional contributions triggered by disorder tend to soften the polarization dependence of the $I^{\parallel}_{\mathrm{THG}}$ signal, irrespective of the pairing symmetry [44–46]. On the other hand, the perpendicular component is expected to still retain the angular dependence of the clean case, at least in the limit where paramagnetic effects are not quantitatively dominant. In this respect, the present calculations performed in the clean limit should remain valid concerning the dependence of $I^{\perp}_{\mathrm{THG}}$ on the gap symmetry, even when one includes realistic disorder effects, which are beyond the scope of the present paper.

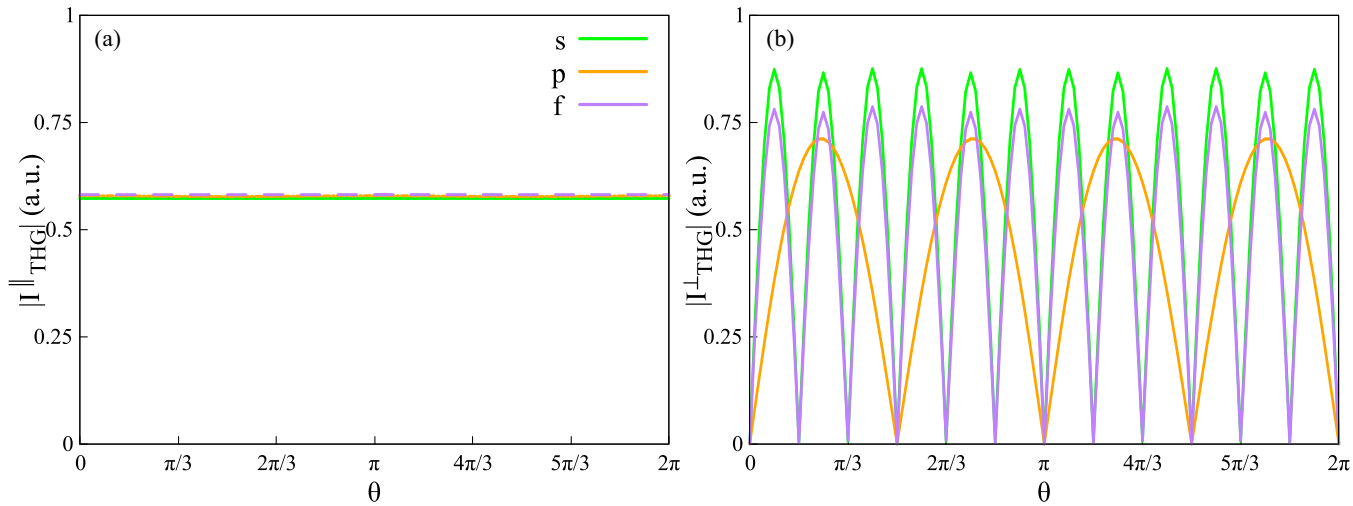


FIG. 4. $I^{\parallel}_{\mathrm{THG}}$(a) and $I^{\perp}_{\mathrm{THG}}$(b) as a function of θ, corresponding to $E_{\mathrm{peak}} = 0.66\ \mathrm{kVcm}^{-1}$ and obtained for the s-wave (green line), p-wave (orange line), and f-wave (purple line) order parameters.

V. DISCUSSION

We study the superconductivity reported recently in the Sn/Si(111) adlayers doped with boron. Assuming that the interactions responsible for the pairing are of AFM nature, we describe the system by the $t-J$ model. Our MF analysis well reproduces the value of the AFM coupling, J, predicted by first-principle calculations and the d-wave symmetry of the SC OP claimed by recent experimental findings [17]. By perturbing the system with an intense THz electromagnetic field, we focus on the leading nonlinear effects, the THG, showing that its dependence on the polarization of the incident field can distinguish between the chiral $d_{x^2-y^2}+id_{xy}$- and the nematic d-wave symmetry of the SC gap, possibly supporting the topological nature of superconductivity in the system under investigation, thus providing insights on the possible existence of zero-energy edge states at the edge of superconducting domains.

However, our results suggest that the periodicity of the THG depends mainly on the discrete symmetries of the modulus of the gap's wave function. We then expect that while the polarization dependence of the THG can successfully distinguish a nematic from a chiral state, it can hardly provide useful information about the angular momentum of the gap's wave function. Nonetheless, as demonstrated by our extended analysis, we find an experimental probe to distinguish triplet-p from triplet -f wave superconductivity and, in general, to access the response of different symmetries of the gap function.

In conclusion, our work (i) provides a minimal efficient theoretical model for describing the pairing in the emerging superconductor Sn/Si(111) and (ii) suggests a powerful experimental method to get insight into the pairing symmetry therein, namely the THz pump protocol, that has succeeded so far in investigating both conventional and high-T_c cuprate superconductors and which can now be extended to include polarization response.

ACKNOWLEDGMENTS

We thank Andrea Marini for helpful and interesting conversations. T.C., C.T., and G.P. acknowledge support from CINECA for computational resources through ISCRA projects. T.C., M.I., G.P., and C.T. acknowledge support from Laboratori Nazionali del Gran Sasso for computational resources. Research at SPIN-CNR has been funded by the European Union - NextGenerationEU under the Italian Ministry of University and Research (MUR) National Innovation Ecosystem Grant No. ECS00000041 - VITALITY; C.T. acknowledges Università degli Studi di Perugia and MUR for support within the project Vitality. C.T. acknowledges financial support from the Italian Ministry for Research and Education through PRIN-2022 project "DARk-mattEr-DEVIces-for-Low-energy-detection - DAREDEVIL" (IT-MIUR Grant No. 2022Z4RARB). L.B. acknowledges financial support by Sapienza University under projects Ateneo (Grants No. RM12117A4A7FD11B and No. RP1221816662A977) and by ICSC–Centro Nazionale di Ricerca in High Performance Computing, Big Data and Quantum Computing, funded by European Union – NextGenerationEU.

G.P. acknowledges financial support by the European Union – NextGenerationEU, Project Code No. PE0000021 - CUP B53C22004060006 - "SUPERMOL," "Network 4 Energy Sustainable Transition – NEST," and the European Union - NextGenerationEU under the Italian Ministry of University and Research (MUR) National Innovation Ecosystem Grant No. ECS00000041 - VITALITY - CUP E13C22001060006.

The authors declare no competing interests.

DATA AVAILABILITY

Data are available in the Supplemental Material and upon request to the contact author.

[1] J. M. Carpinelli, H. H. Weitering, E. W. Plummer, and R. Stumpf, Direct observation of a surface charge density wave, Nature (London) **381**, 398 (1996).

[2] G. Santoro, S. Scandolo, and E. Tosatti, Charge-density waves and surface Mott insulators for adlayer structures on semiconductors: Extended Hubbard modeling, Phys. Rev. B **59**, 1891 (1999).

[3] R. Cortés, A. Tejeda, J. Lobo-Checa, C. Didiot, B. Kierren, D. Malterre, J. Merino, F. Flores, E. G. Michel, and A. Mascaraque, Competing charge ordering and Mott phases in a correlated Sn/Ge(111) two-dimensional triangular lattice, Phys. Rev. B **88**, 125113 (2013).

[4] P. Hansmann, T. Ayral, L. Vaugier, P. Werner, and S. Biermann, Long-range Coulomb interactions in surface systems: A first-principles description within self-consistently combined *GW* and dynamical mean-field theory, Phys. Rev. Lett. **110**, 166401 (2013).

[5] D. I. Badrtdinov, S. A. Nikolaev, M. I. Katsnelson, and V. V. Mazurenko, Spin-orbit coupling and magnetic interactions in Si(111):C,Si,Sn,Pb, Phys. Rev. B **94**, 224418 (2016).

[6] C. Tresca, C. Brun, T. Bilgeri, G. Menard, V. Cherkez, R. Federicci, D. Longo, F. Debontridder, M. D'angelo, D. Roditchev, G. Profeta, M. Calandra, and T. Cren, Chiral spin texture in the charge-density-wave phase of the correlated metallic Pb/Si(111) monolayer, Phys. Rev. Lett. **120**, 196402 (2018).

[7] F. Adler, S. Rachel, M. Laubach, J. Maklar, A. Fleszar, J. Schäfer, and R. Claessen, Correlation-driven charge order in a frustrated two-dimensional atom lattice, Phys. Rev. Lett. **123**, 086401 (2019).

[8] C. Tresca and M. Calandra, Charge density wave in single-layer Pb/Ge(111) driven by Pb-substrate exchange interaction, Phys. Rev. B **104**, 045126 (2021).

[9] C. Tresca, T. Bilgeri, G. Ménard, V. Cherkez, R. Federicci, D. Longo, M. Hervé, F. Debontridder, P. David, D. Roditchev, G. Profeta, T. Cren, M. Calandra, and C. Brun, Importance of accurately measuring LDOS maps using scanning tunneling spectroscopy in materials presenting atom-dependent charge order: The case of the correlated Pb/Si(111) single atomic layer, Phys. Rev. B **107**, 035125 (2023).

[10] G. Profeta and E. Tosatti, Triangular Mott-Hubbard insulator phases of Sn/Si(111) and Sn/Ge(111) surfaces, Phys. Rev. Lett. **98**, 086401 (2007).

[11] M. Iannetti, S. Modesti, G. Di Santo, M. Caputo, P. M. Sheverdyaeva, P. Moras, F. Chiapolino, T. Cea, C. Tresca, E. Tosatti, *et al.*, Electronic structure of a doped Mott-Hubbard surface, Phys. Rev. B **112**, 075159 (2025).

[12] G. Li, P. Höpfner, J. Schäfer, C. Blumenstein, S. Meyer, A. Bostwick, E. Rotenberg, R. Claessen, and W. Hanke, Magnetic order in a frustrated two-dimensional atom lattice at a semiconductor surface, Nat. Commun. **4**, 1620 (2013).

[13] J.-H. Lee, X.-Y. Ren, Y. Jia, and J.-H. Cho, Antiferromagnetic superexchange mediated by a resonant surface state in Sn/Si(111), Phys. Rev. B **90**, 125439 (2014).

[14] X. Wu, F. Ming, T. S. Smith, G. Liu, F. Ye, K. Wang, S. Johnston, and H. H. Weitering, Superconductivity in a hole-doped Mott-insulating triangular adatom layer on a silicon surface, Phys. Rev. Lett. **125**, 117001 (2020).

[15] S. Wolf, D. Di Sante, T. Schwemmer, R. Thomale, and S. Rachel, Triplet superconductivity from nonlocal Coulomb repulsion in an atomic Sn layer deposited onto a Si(111) substrate, Phys. Rev. Lett. **128**, 167002 (2022).

[16] M. Biderang, M.-H. Zare, and J. Sirker, Topological superconductivity in Sn/Si(111) driven by nonlocal Coulomb interactions, Phys. Rev. B **106**, 054514 (2022).

[17] F. Ming, X. Wu, C. Chen, K. D. Wang, P. Mai, T. A. Maier, J. Strockoz, J. W. F. Venderbos, C. González, J. Ortega, S. Johnston, and H. H. Weitering, Evidence for chiral superconductivity on a silicon surface, Nat. Phys. **19**, 500 (2023).

[18] M. Zahedifar and P. Kratzer, Phonon-induced electronic relaxation in a strongly correlated system: The Sn/Si(111) ($\sqrt{3} \times \sqrt{3}$) adlayer revisited, Phys. Rev. B **100**, 125427 (2019).

[19] L. Marchetti, M. Bunney, D. Di Sante, and S. Rachel, Electronic structure, spin-orbit interaction, and electron-phonon coupling of triangular adatom lattices on semiconductor substrates, Phys. Rev. B **111**, 125115 (2025).

[20] R. Nandkishore, L. S. Levitov, and A. V. Chubukov, Chiral superconductivity from repulsive interactions in doped graphene, Nat. Phys. **8**, 158 (2012).

[21] M. L. Kiesel, C. Platt, W. Hanke, D. A. Abanin, and R. Thomale, Competing many-body instabilities and unconventional superconductivity in graphene, Phys. Rev. B **86**, 020507(R) (2012).

[22] M. L. Kiesel, C. Platt, W. Hanke, and R. Thomale, Model evidence of an anisotropic chiral $d+id$-wave pairing state for the water-intercalated $Na_xCoO_2 \cdot y\mathbf{H_2O}$ superconductor, Phys. Rev. Lett. **111**, 097001 (2013).

[23] Y. Huang, S.-S. Gong, and D. N. Sheng, Quantum phase diagram and spontaneously emergent topological chiral superconductivity in doped triangular-lattice Mott insulators, Phys. Rev. Lett. **130**, 136003 (2023).

[24] Y. Huang and D. N. Sheng, Topological chiral and nematic superconductivity by doping Mott insulators on triangular lattice, Phys. Rev. X **12**, 031009 (2022).

[25] D. Nicoletti and A. Cavalleri, Nonlinear light–matter interaction at terahertz frequencies, Adv. Opt. Photon. **8**, 401 (2016).

[26] R. Shimano and N. Tsuji, Higgs mode in superconductors, Annu. Rev. Condens. Matter Phys. **11**, 103 (2020).

[27] C.-J. Yang, J. Li, M. Fiebig, and S. Pal, Terahertz control of many-body dynamics in quantum materials, Nat. Rev. Mater. **8**, 518 (2023).

[28] R. Matsunaga, N. Tsuji, H. Fujita, A. Sugioka, K. Makise, Y. Uzawa, H. Terai, Z. Wang, H. Aoki, and R. Shimano, Light-induced collective pseudospin precession resonating with Higgs mode in a superconductor, Science **345**, 1145 (2014).

[29] R. Matsunaga, N. Tsuji, K. Makise, H. Terai, H. Aoki, and R. Shimano, Polarization-resolved terahertz third-harmonic generation in a single-crystal superconductor NbN: Dominance of the Higgs mode beyond the BCS approximation, Phys. Rev. B **96**, 020505(R) (2017).

[30] K. Katsumi, N. Tsuji, Y. I. Hamada, R. Matsunaga, J. Schneeloch, R. D. Zhong, G. D. Gu, H. Aoki, Y. Gallais, and R. Shimano, Higgs mode in the d-wave superconductor $Bi_2Sr_2CaCu_2O_{8+x}$ driven by an intense terahertz pulse, Phys. Rev. Lett. **120**, 117001 (2018).

[31] X. Yang, C. Vaswani, C. Sundahl, M. Mootz, P. Gagel, L. Luo, J. H. Kang, P. P. Orth, I. E. Perakis, C. B. Eom, and J. Wang, Terahertz-light quantum tuning of a metastable emergent phase hidden by superconductivity, Nat. Mater. **17**, 586 (2018).

[32] F. Giorgianni, T. Cea, C. Vicario, C. P. Hauri, W. K. Withanage, X. Xi, and L. Benfatto, Leggett mode controlled by light pulses, Nat. Phys. **15**, 341 (2019).

[33] X. Yang, C. Vaswani, C. Sundahl, M. Mootz, L. Luo, J. H. Kang, I. E. Perakis, C. B. Eom, and J. Wang, Lightwave-driven gapless superconductivity and forbidden quantum beats by terahertz symmetry breaking, Nat. Photon. **13**, 707 (2019).

[34] H. Chu, M.-J. Kim, K. Katsumi, S. Kovalev, R. D. Dawson, L. Schwarz, N. Yoshikawa, G. Kim, D. Putzky, Z. Z. Li, H. Raffy, S. Germanskiy, J.-C. Deinert, N. Awari, I. Ilyakov, B. Green, M. Chen, M. Bawatna, G. Cristiani, G. Logvenov, *et al.*, Phase-resolved Higgs response in superconducting cuprates, Nat. Commun. **11**, 1793 (2020).

[35] K. Katsumi, Z. Z. Li, H. Raffy, Y. Gallais, and R. Shimano, Superconducting fluctuations probed by the Higgs mode in $Bi_2Sr_2CaCu_2O_{8+x}$ thin films, Phys. Rev. B **102**, 054510 (2020).

[36] K. Isoyama, N. Yoshikawa, K. Katsumi, J. Wong, N. Shikama, Y. Sakishita, F. Nabeshima, A. Maeda, and R. Shimano, Light-induced enhancement of superconductivity in iron-based superconductor $FeSe_{0.5}Te_{0.5}$, Commun. Phys. **4**, 160 (2021).

[37] S. Kovalev, T. Dong, L.-Y. Shi, C. Reinhoffer, T.-Q. Xu, H.-Z. Wang, Y. Wang, Z.-Z. Gan, S. Germanskiy, J.-C. Deinert, I. Ilyakov, P. H. M. van Loosdrecht, D. Wu, N.-L. Wang, J. Demsar, and Z. Wang, Band-selective third-harmonic generation in superconducting MgB_2: Possible evidence for the Higgs amplitude mode in the dirty limit, Phys. Rev. B **104**, L140505 (2021).

[38] Z.-X. Wang, J.-R. Xue, H.-K. Shi, X.-Q. Jia, T. Lin, L.-Y. Shi, T. Dong, F. Wang, and N.-L. Wang, Transient Higgs oscillations and high-order nonlinear light-Higgs coupling in a terahertz wave driven NbN superconductor, Phys. Rev. B **105**, L100508 (2022).

[39] C. Reinhoffer, P. Pilch, A. Reinold, P. Derendorf, S. Kovalev, J.-C. Deinert, I. Ilyakov, A. Ponomaryov, M. Chen, T.-Q. Xu, Y. Wang, Z.-Z. Gan, D.-S. Wu, J.-L. Luo, S. Germanskiy, E. A. Mashkovich, P. H. M. van Loosdrecht, I. M. Eremin, and Z. Wang, High-order nonlinear terahertz probing of the two-band superconductor MgB_2: Third- and fifth-order harmonic generation, Phys. Rev. B **106**, 214514 (2022).

[40] L. Luo, M. Mootz, J. H. Kang, C. Huang, K. Eom, J. W. Lee, C. Vaswani, Y. G. Collantes, E. E. Hellstrom, I. E. Perakis, C. B. Eom, and J. Wang, Quantum coherence tomography of light-controlled superconductivity, Nat. Phys. **19**, 201 (2023).

[41] H. Chu, S. Kovalev, Z. X. Wang, L. Schwarz, T. Dong, L. Feng, R. Haenel, M.-J. Kim, P. Shabestari, L. P. Hoang, K. Honasoge, R. D. Dawson, D. Putzky, G. Kim, M. Puviani, M. Chen, N. Awari, A. N. Ponomaryov, I. Ilyakov, M. Bluschke, *et al.*, Fano interference between collective modes in cuprate high-Tc superconductors, Nat. Commun. **14**, 1343 (2023).

[42] M.-J. Kim, S. Kovalev, M. Udina, R. Haenel, G. Kim, M. Puviani, G. Cristiani, I. Ilyakov, T. V. A. G. de Oliveira, A. Ponomaryov, J.-C. Deinert, G. Logvenov, B. Keimer, D. Manske, L. Benfatto, and S. Kaiser, Tracing the dynamics of superconducting order via transient terahertz third-harmonic generation, Sci. Adv. **10**, eadi7598 (2024).

[43] T. Cea, P. Barone, C. Castellani, and L. Benfatto, Polarization dependence of the third-harmonic generation in multiband superconductors, Phys. Rev. B **97**, 094516 (2018).

[44] G. Seibold, M. Udina, C. Castellani, and L. Benfatto, Third harmonic generation from collective modes in disordered superconductors, Phys. Rev. B **103**, 014512 (2021).

[45] M. Udina, J. Fiore, T. Cea, C. Castellani, G. Seibold, and L. Benfatto, THz non-linear optical response in cuprates: Predominance of the BCS response over the Higgs mode, Faraday Discuss. **237**, 168 (2022).

[46] L. Benfatto, C. Castellani, and G. Seibold, Linear and nonlinear current response in disordered d-wave superconductors, Phys. Rev. B **108**, 134508 (2023).

[47] L. Schwarz, B. Fauseweh, N. Tsuji, N. Cheng, N. Bittner, H. Krull, M. Berciu, G. S. Uhrig, A. P. Schnyder, S. Kaiser, and D. Manske, Classification and characterization of nonequilibrium Higgs modes in unconventional superconductors, Nat. Commun. **11**, 287 (2020).

[48] K. Katsumi, M. Nishida, S. Kaiser, S. Miyasaka, S. Tajima, and R. Shimano, Near-infrared light-induced superconducting-like state in underdoped $YBa_2Cu_3O_y$ studied by c-axis terahertz third-harmonic generation, Phys. Rev. B **107**, 214506 (2023).

[49] B. A. Levitan, J. Eid, and T. Pereg-Barnea, Signatures of the order parameter of a superconducting adatom layer in magnetic field dependent quasiparticle interference, Phys. Rev. B **107**, 174504 (2023).

[50] See Supplemental Material at http://link.aps.org/supplemental/10.1103/p357-5pth for the tight-binding parameters used for the calculations; the noninteracting band structure; the derivation of the mean-field Hamiltonian; the fit of the mean-field exchange constant; the figure of the mean-field solutions; and the discussion on the symmetry of the gap function.

[51] P. W. Anderson, The resonating valence bond state in La_2CuO_4 and superconductivity, Science **235**, 1196 (1987).

[52] P. A. Lee, N. Nagaosa, and X.-G. Wen, Doping a Mott insulator: Physics of high-temperature superconductivity, Rev. Mod. Phys. **78**, 17 (2006).

[53] M. Ogata and H. Fukuyama, The t–j model for the oxide high-Tc superconductors, Rep. Prog. Phys. **71**, 036501 (2008).

[54] B. Keimer, S. A. Kivelson, M. R. Norman, S. Uchida, and J. Zaanen, From quantum matter to high-temperature superconductivity in copper oxides, Nature (London) **518**, 179 (2015).

[55] E. Fradkin, S. A. Kivelson, and J. M. Tranquada, *Colloquium*: Theory of intertwined orders in high temperature superconductors, Rev. Mod. Phys. **87**, 457 (2015).

[56] C. Proust and L. Taillefer, The remarkable underlying ground states of cuprate superconductors, Annu. Rev. Condens. Matter Phys. **10**, 409 (2019).

[57] D. P. Arovas, E. Berg, S. A. Kivelson, and S. Raghu, The Hubbard model, Annu. Rev. Condens. Matter Phys. **13**, 239 (2022).

[58] C. Honerkamp, Instabilities of interacting electrons on the triangular lattice, Phys. Rev. B **68**, 104510 (2003).

[59] Q.-H. Wang, D.-H. Lee, and P. A. Lee, Doped $t-j$ model on a triangular lattice: Possible application to $Na_xCoO_2 \cdot yH_2O$ and $Na_{1-x}TiO_2$, Phys. Rev. B **69**, 092504 (2004).

[60] B. Kumar and B. S. Shastry, Superconductivity in CoO_2 layers and the resonating valence bond mean-field theory of the triangular lattice $t-j$ model, Phys. Rev. B **68**, 104508 (2003).

[61] G. Baskaran, Electronic model for CoO_2 layer based systems: Chiral resonating valence bond metal and superconductivity, Phys. Rev. Lett. **91**, 097003 (2003).

[62] L. Classen, C. Honerkamp, and M. M. Scherer, Competing phases of interacting electrons on triangular lattices in moiré heterostructures, Phys. Rev. B **99**, 195120 (2019).

[63] S. Raghu, S. A. Kivelson, and D. J. Scalapino, Superconductivity in the repulsive Hubbard model: An asymptotically exact weak-coupling solution, Phys. Rev. B **81**, 224505 (2010).

[64] Y.-F. Jiang and H.-C. Jiang, Topological superconductivity in the doped chiral spin liquid on the triangular lattice, Phys. Rev. Lett. **125**, 157002 (2020).

[65] V. Blum, R. Gehrke, F. Hanke, P. Havu, V. Havu, X. Ren, K. Reuter, and M. Scheffler, *Ab initio* molecular simulations with numeric atom-centered orbitals, Comput. Phys. Commun. **180**, 2175 (2009).

[66] X. Ren, P. Rinke, V. Blum, J. Wieferink, A. Tkatchenko, A. Sanfilippo, K. Reuter, and M. Scheffler, Resolution-of-identity approach to Hartree–Fock, hybrid density functionals, RPA, MP2 and GW with numeric atom-centered orbital basis functions, New J. Phys. **14**, 053020 (2012).

[67] J. Heyd, G. E. Scuseria, and M. Ernzerhof, Hybrid functionals based on a screened Coulomb potential, J. Chem. Phys. **118**, 8207 (2003).

[68] J. Heyd, G. E. Scuseria, and M. Ernzerhof, Erratum: "Hybrid functionals based on a screened Coulomb potential" [J. Chem. Phys. **118**, 8207 (2003)], J. Chem. Phys. **124**, 219906(E) (2006).

[69] J. Lobo, A. Tejeda, A. Mugarza, and E. G. Michel, Electronic structure of Sn/Si (111) $-(\sqrt{3}\times\sqrt{3})R30°$ as a function of Sn coverage, Phys. Rev. B **68**, 235332 (2003).

[70] H. Nishimichi, T. Machida, S. Ichinokura, S. Kaku, K. Ishihara, K. Tanaka, T. Hanaguri, and T. Hirahara, Momentum-resolved spectroscopic evidence of a metal-insulator transition in Si (111) 3× 3-Sn, Phys. Rev. B **111**, 235134 (2025).

[71] S. Modesti, L. Petaccia, G. Ceballos, I. Vobornik, G. Panaccione, G. Rossi, L. Ottaviano, R. Larciprete, S. Lizzit, and A. Goldoni, Insulating ground state of Sn/Si (111) $-(\sqrt{3}\times\sqrt{3})R30°$, Phys. Rev. Lett. **98**, 126401 (2007).

[72] L. Ottaviano, M. Crivellari, L. Lozzi, and S. Santucci, STM investigation of the α-Sn/Si (111) phase at 120 K, Surf. Sci. **445**, L41 (2000).

[73] H. Morikawa, I. Matsuda, and S. Hasegawa, STM observation of Si (111)-$\alpha - 3\times$ 3-Sn at low temperature, Phys. Rev. B **65**, 201308(R) (2002).

[74] M. Jäger, C. Brand, A. P. Weber, M. Fanciulli, J. H. Dil, H. Pfnür, and C. Tegenkamp, α-Sn phase on Si (111): Spin texture of a two-dimensional Mott state, Phys. Rev. B **98**, 165422 (2018).

[75] C. Vaswani, M. Mootz, C. Sundahl, D. Mudiyanselage, J. Kang, X. Yang, D. Cheng, C. Huang, R. Kim, Z. Liu, *et al.*, Terahertz second-harmonic generation from lightwave acceleration of symmetry-breaking nonlinear supercurrents, Phys. Rev. Lett. **124**, 207003 (2020).

[76] M. Silaev, Nonlinear electromagnetic response and Higgs-mode excitation in BCS superconductors with impurities, Phys. Rev. B **99**, 224511 (2019).

[77] N. Tsuji and Y. Nomura, Higgs-mode resonance in third harmonic generation in NbN superconductors: Multiband electron-phonon coupling, impurity scattering, and polarization-angle dependence, Phys. Rev. Res. **2**, 043029 (2020).

Correction: The author order was incorrect and has been fixed, which necessitated a change in the affiliation setup.